The interaction of aromatic molecules with the acid site in zeolite H-Beta as observed through a newly discovered Fano resonance at the Al K edge

2001 J. Phys.: Condens. Matter 13 10383

(http://iopscience.iop.org/0953-8984/13/46/310)

INSTITUTE OF PHYSICS PUBLISHING JOURNAL OF PHYSICS: CONDENSED MATTER

J. Phys.: Condens. Matter **13** (2001) 10383–10398 PII: S0953-8984(01)24895-4

The interaction of aromatic molecules with the acid site in zeolite H-Beta as observed through a newly discovered Fano resonance at the Al K edge

J A van Bokhoven[1,3], D C Koningsberger[1] and D E Ramaker[2]

[1] Debye Institute, Department of Inorganic Chemistry and Catalysis, Utrecht University, Sorbonnelaan 16, 3584 CH Utrecht, The Netherlands
[2] Chemistry Department, George Washington University, Washington, DC 20052, USA

E-mail: J.A.vanBokhoven@chem.uu.nl

Received 16 May 2001, in final form 16 August 2001
Published 2 November 2001
Online at stacks.iop.org/JPhysCM/13/10383

Abstract

A new tool to study the interaction of aromatic molecules with the acid sites in zeolites is described yielding both geometric and electronic information simultaneously. A Fano resonance (or two-centre/two-electron transition state) produces a charge-transfer (CT) satellite peak that is observed in the Al K edge XANES of zeolite H-Beta when aromatic hydrocarbon molecules are adsorbed on its acid sites. The Fano resonance is exclusively observed in the electron yield spectrum. The Fano resonance can be recognized as a broad, featureless satellite peak at a somewhat higher energy than the edge. During the 1s–3p transition, a CT occurs from π orbitals on the aromatic molecule to the T_2 (3p) orbital on the Al transferring charge from the benzene to the aluminium. The diffuse character of this latter orbital results in an overlap with the π^* of the aromatics and enables the CT. FEFF8 FMS and DOS calculations on a large cluster representing the zeolite with and without benzene and in the presence and absence of the core hole effect confirm the satellite interpretation.

The Fano resonance satellite is not observed in the fluorescence detection mode, because its inherent excitation probability is small, but its intensity is magnified in the electron yield detection mode because of shake-off of the extra Al valence electrons. The data indicate that the adsorbates do not alter the symmetry of the tetrahedral Al sites as indicated by both fluorescence and electron yield.

The adsorption of 1-hexene on zeolite H-Beta is investigated and only after a heat treatment of 400 °C is the Fano transition visible. This indicates that aromatic coke has formed on the acid site at this temperature. In addition, some transformation from tetrahedral Al sites into octahedral sites, or at least some geometric distortion of a small amount of tetrahedral Al sites, is now observed in the fluorescence spectrum, which might be induced by the coking process.

[3] Corresponding author.

1. Introduction

Zeolites have a major application among others in catalysis as catalysts and catalyst supports, or as a sorption reagent [1]. The structure of the zeolite has a strong influence on its efficiency in the applications mentioned. Thus many studies have been reported relating the structure of the zeolite to its catalytic activity, sorption capacity, and sorbent diffusion in the pores of zeolites.

Al K edge XANES provides information about the local coordination of Al in the samples studied. The near edge can be used as a fingerprint for the determination of the Al coordination [2, 3]. Moreover, some authors have tried to interpret the data on a molecular orbital level [4–6]. Although considerable controversy over the source of some peaks in the spectra still exists, these studies have significantly increased the insight into the source of the features in the spectra.

In this study, the adsorption of hydrocarbons on the acid sites of zeolite Beta is investigated by Al K edge XANES. A unique two-centre, two-electron transition is described, that is primarily detected as a satellite feature or Fano resonance, whose intensity gets magnified in electron yield mode. The transition involves the normal Al 1s to 3p XAS excitation simultaneous with a π (orbital on the aromatic hydrocarbon) to π^* (overlapping the Al 3p) charge transfer (CT) to screen the core hole. As a two-electron transition, it represents a true Fano resonance in the continuum, rather than the more frequently observed one-electron shape resonance involving an antibonding orbital in the continuum. This satellite feature provides a new tool to study adsorption of aromatic molecules on zeolites. We use 1-hexene coking on H-Beta as an example.

2. Experiment

Zeolite NH_4 Beta was obtained from TUD and has a reported Si/Al ratio of 11.6. The average crystal size is $\sim$0.2 μm determined by TEM. This sample is calcined at 1 °C min^{-1} to 450 °C, and kept at 450 °C for 8 h in order to remove NH_3. This sample is referred to as H-Beta. The H-Beta is then loaded with adsorbate by saturating the powder at RT by liquid benzene (p.a. Merck) and 1-hexene (97%, Acros), respectively. The samples are completely wetted in the liquids by using about twice the volume of liquid compared to the volume of the zeolite. Samples are dried overnight at room temperature in dry nitrogen. The samples are called H-Beta/benzene and H-Beta/1-hexene. H-Beta/1-hexene is subsequently heated at a rate of 1 °C min^{-1} to 250 °C in a flow of dry nitrogen (40 ml min^{-1}) nitrogen for 1 h under shallow bed conditions; this sample is called H-Beta/1-hexene(250). Another batch is heated to 400 °C at the same heating rate for 1 h. This sample is called H-Beta/1-hexene(400). All samples are white, except H-Beta/1-hexene(250) and H-Beta/1-hexene(400), which are beige and brownish grey coloured, respectively. Samples are pressed by hand into a wafer onto a carbon adhesive tab before measurement. ^{13}C NMR on H-Beta with adsorbed benzene and subsequent heating at 75 °C in vacuum shows the spectrum of benzene, but the peaks are broadened.

The measurements have been performed in the newly designed *in situ* apparatus, ILEXAFS, *in situ* low energy x-ray absorption fine structure, which has been installed at beamline 3.4 at the SRS Daresbury (UK) [7, 8]. Fluorescence (using a gas proportional counter) and electron yield (measuring drain current) data have been collected simultaneously. Dilution of the samples with carbon did not show significantly better electron yield spectra, hence no carbon-dilution is used. During measurement, the samples are cooled down to liquid nitrogen temperature.

In order to interpret the Fano resonance on a molecular orbital level, FEFF8 [9] full multiple scattering (FMS) and DOS calculations have been performed on a cluster representing the zeolite. The output of such calculations is (among other things) the FMS and the DOS. In the calculations, the Hedin Lunqvist potential is used and self-consistent field (SCF) calculations have been performed. To investigate the effect of any screening of the core hole on the shape of the DOS, calculations in the presence and absence of the core hole are performed.

The cluster used is generated by CERIUS2 by cutting a cluster, $AlSi_{29}O_{74}(H)$, from the crystallographic structure of zeolite Beta with the aluminium atom in the centre of the cluster. A benzene molecule was placed on the acidic site to mimic the adsorbed state. After a geometry optimization of the benzene (using a force field in the commercial CERIUS2 package) keeping the zeolite cluster fixed the Cartesian coordinates were obtained. The nearest Al–C and O–C distances are 3.2 and 2.1 Å, respectively. Essentially, the plane of the benzene molecule is positioned perpendicular to the O–H bond.

3. Results

Figure 1 shows the electron yield (bottom) and fluorescence yield (top) Al K-edge XANES spectra of H-Beta. Both spectra display very similar features; however, the white line in the fluorescence yield is reduced. This is attributed to the self-absorption of the fluorescence radiation by the sample, which is especially important at the white line. Both spectra show the well known characteristic features of a tetrahedrally coordinated aluminum ion [2], indicating the sample contains primarily tetrahedral Al: the sharp white line is positioned at 1567 eV and a broad peak at ∼1585 eV (∼20 eV above the edge) is visible. Moreover, in the energy range 0–15 eV above the edge, fine structure characteristic of tetrahedral Al is visible. The 20 eV peak has been assigned to a p–d hybridized anti-bonding σ^* orbital, whose p character is probed in the K-edge spectra [5]. The spectral lineshape of this peak is primarily determined by multiple scattering in the first coordination sphere of tetrahedral Al, and its energy is a strong function of the Al–O bond length. The intensity in the 0–15 eV region corresponds to the p character in a p–d hybridized orbital and the fine structure in this region is mainly determined by longer range multiple scattering (up to 15 Å about the absorber) [4,5,10]. Based on ^{27}Al MAS NMR and Al K-edge XANES, the presence of a small fraction of octahedral Al in (macro-crystalline) H-Beta was proven [11].

Figure 2 shows the fluorescence and electron yield spectrum of H-Beta/benzene. The fluorescence spectrum is very similar to the spectrum of clean H-Beta (figure 1) indicating no changes in the Al coordination. The spectrum as detected by electron yield displays remarkable differences that are to our knowledge unreported in the literature. The electron yield spectrum of H-Beta/benzene is completely dominated by a broad peak at ∼5 eV above the absorption edge. The broad peak at ∼20 eV is still present and its intensity is essentially unaffected compared to the intensity of the 20 eV peak in the electron yield spectrum of H-Beta. At 1567 eV, a shoulder on the rising edge of the broad dominating peak is clearly visible.

The fluorescence yield spectra in figure 3(*a*) for H-Beta/1-hexene and H-Beta/1-hexene(250) are very similar to the spectrum of H-Beta. The spectrum of H-Beta/1-hexene(400) reveals a slight loss of intensity in the white line at 1567 eV compared to the other two and an increase in intensity at ∼7 eV above the edge. Further, the fine structure in the 5–15 eV region above the edge is significantly less distinct. The electron yield spectra of H-Beta/1-hexene, H-Beta/1-hexene(250) and H-Beta/1-hexene(400) are shown in figure 3(*b*). The spectrum of H-Beta/1-hexene is noisy, but it still reveals a sharp white line, and a broad peak at ∼20 eV. The white line seems to be diminished in intensity, but the poor quality of the data does not permit us to draw firm conclusions. The spectra of H-Beta/1-hexene and

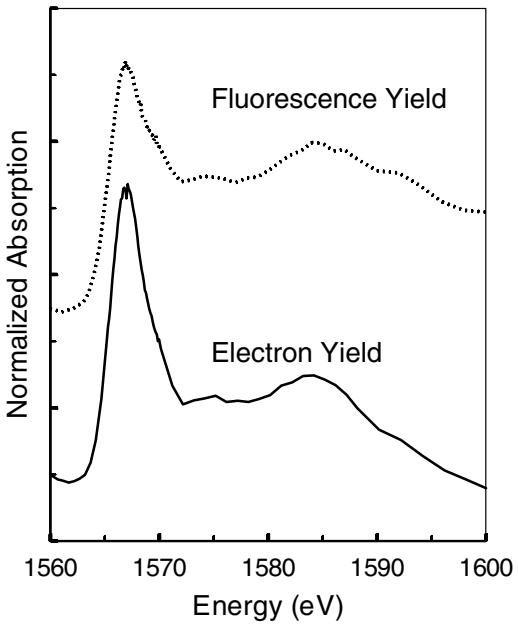

Figure 1. Al K-edge XANES spectrum of H-Beta as measured by electron yield (bottom) and fluorescence yield detection. These spectra indicate a tetrahedral Al coordination.

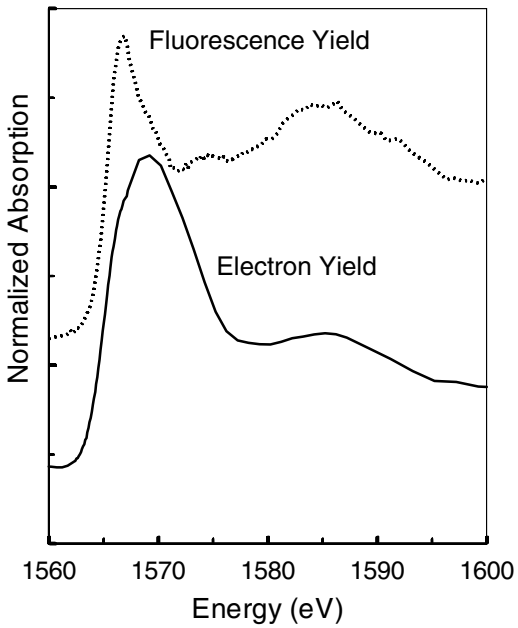

Figure 2. Fluorescence yield and electron yield detected spectra of H-Beta/benzene showing striking differences between the two detection methods.

H-Beta/1-hexene(250) are very similar and do not differ from the electron yield spectrum of 'clean' H-Beta (figure 1 (bottom)). The spectrum of H-Beta/1-hexene(400), however, shows a broad resonance that is dominating the edge, like in the spectrum of H-Beta/benzene. The white line at 1567 eV can still be distinguished, and the σ^* peak at 20 eV remains nearly constant in position and intensity.

Figure 4 shows the results of FEFF8 calculations showing the calculated Al K XAS spectra plus the indicated DOS on the $AlSi_{29}O_{74}$ cluster representing the zeolite with and

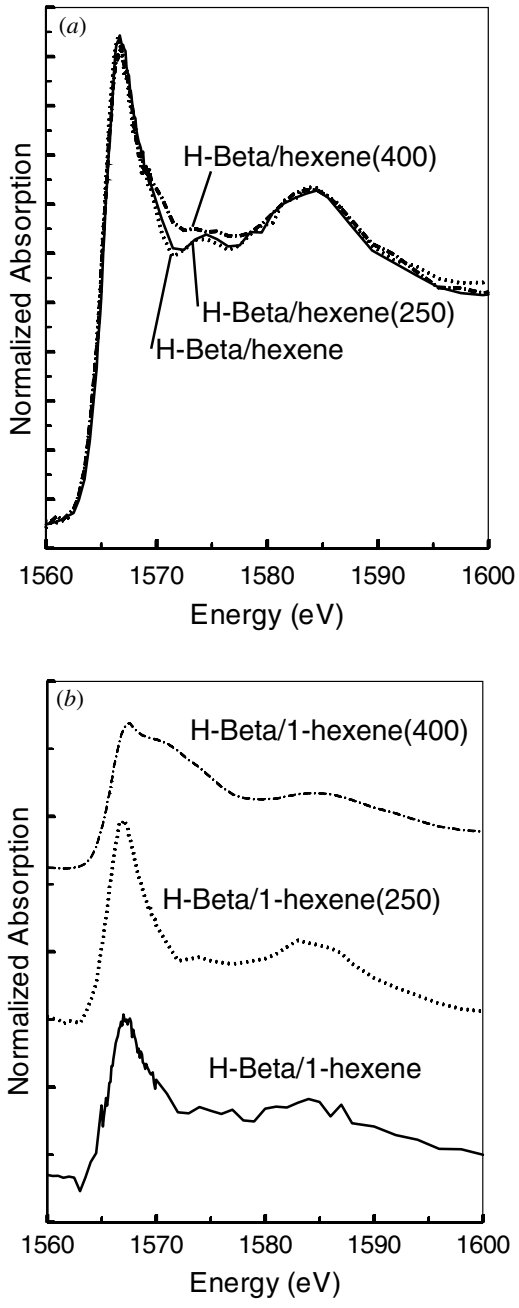

Figure 3. Fluorescence yield (*a*) and electron yield (*b*) detected spectra of H-Beta/1-hexene, H-Beta/1-hexene(250) and H-Beta/1-hexene(400). The latter spectrum differs from the other two by a surplus in intensity in the 3–7 eV range. The electron yield spectrum of H-Beta/1-hexene shows more noise, probably because this sample is less conductive than the others.

without adsorbed benzene. Figure 4(*a*) gives the p DOS on the cluster without benzene by a solid line, in the presence of the core hole. Clearly visible is the correspondence between the Al 3p DOS with the calculated XAS, that have essentially an identical shape. Moreover, a clear agreement with experiment is visible (compare figures 1–4). In [5] these calculations are discussed in more detail. The figure shows the calculated XAS on the same cluster with the benzene on the acid site by the dotted curve. This calculation has been performed again

in the presence of the core hole. The influence of the presence of benzene on the spectrum, although small is discernable. This indicates a direct interaction of the Al p DOS with the benzene. The calculated p DOS on the carbon atoms has been added (dash–dotted curve) in figure 4 showing the relative energy positions of the benzene π and π^* orbitals, and the near degeneracy of the π^* and Al 3p orbitals allowing for reasonable mixing of these two orbitals.

The calculation of the cluster containing benzene, but without the presence of the core hole is shown in figure 4(*b*). The shape of the Al 3p DOS alters dramatically and a shift to higher energy of the bottom of the p DOS occurs. The shape at higher energies is much less affected by the absence of the core hole.

4. Discussion

4.1. Interpretation of differences in fluorescence and electron yield detection

Several reasons for differences in the XANES spectra using fluorescence and electron yield detection are possible and are discussed in this section. The additional broad peak in the electron yield spectra upon molecular adsorption will be assigned to a satellite feature or Fano resonance.

4.2. Surface sensitivity

Differences in the electron and fluorescence yield spectra could result from the different surface sensitivities of these techniques; however, this cannot explain the observed differences in figures 1–3. The zeolite Beta consists of small crystallites that average about 0.2 μm. The penetration depth of fluorescence radiation is of the order of micrometres, whereas the probing depth of the electron yield (drain current) is about 130 Å for Al_2O_3 [12]. Thus the fluorescence yield is expected to probe all of the Al atoms, and the electron yield would probe the Al atoms in the outer 'skin', i.e. just those in the outer 130 Å, which is still $\sim$15% of the total Al atoms. The molecular adsorption does not just take place at the outer surface of the zeolite sample [13]. Thus both the electron yield and fluorescence yield spectra are sampling all or part of the absorbate region.

One might suggest that even though the adsorbates diffuse throughout the zeolite crystallite, the external surface (or near surface) Al atoms might somehow be different than the bulk Al atoms (at the micropore surface). But the electron yield samples 130 Å, far more than just the external surface region. The external surface region is thus a small fraction of the outer 'skin' sampled by the electron yield spectra, even though this fraction is much larger than in the fluorescence yield. Moreover, we estimate that the electron yield technique samples $\sim$15% of the total zeolite crystallite, which is sampled in the fluorescence yield. If the broad and intense 5 eV peak seen in the electron yield spectra were equally present in both techniques, but somehow only produced by Al atoms in the outer 130 Å 'skin', it should still be visible in the fluorescence yield spectra, which it is not. Thus, the difference between the two techniques is due to intrinsic differences in the detection methods.

4.3. Identical Al coordinations in all samples

The very similar fluorescence spectra of all samples indicates that the average coordination of Al in all samples is still predominantly tetrahedral, exactly like that in the parent sample, H-Beta (see the results section). H-Beta/1-hexene(400) is an exception to this, and it is discussed separately.

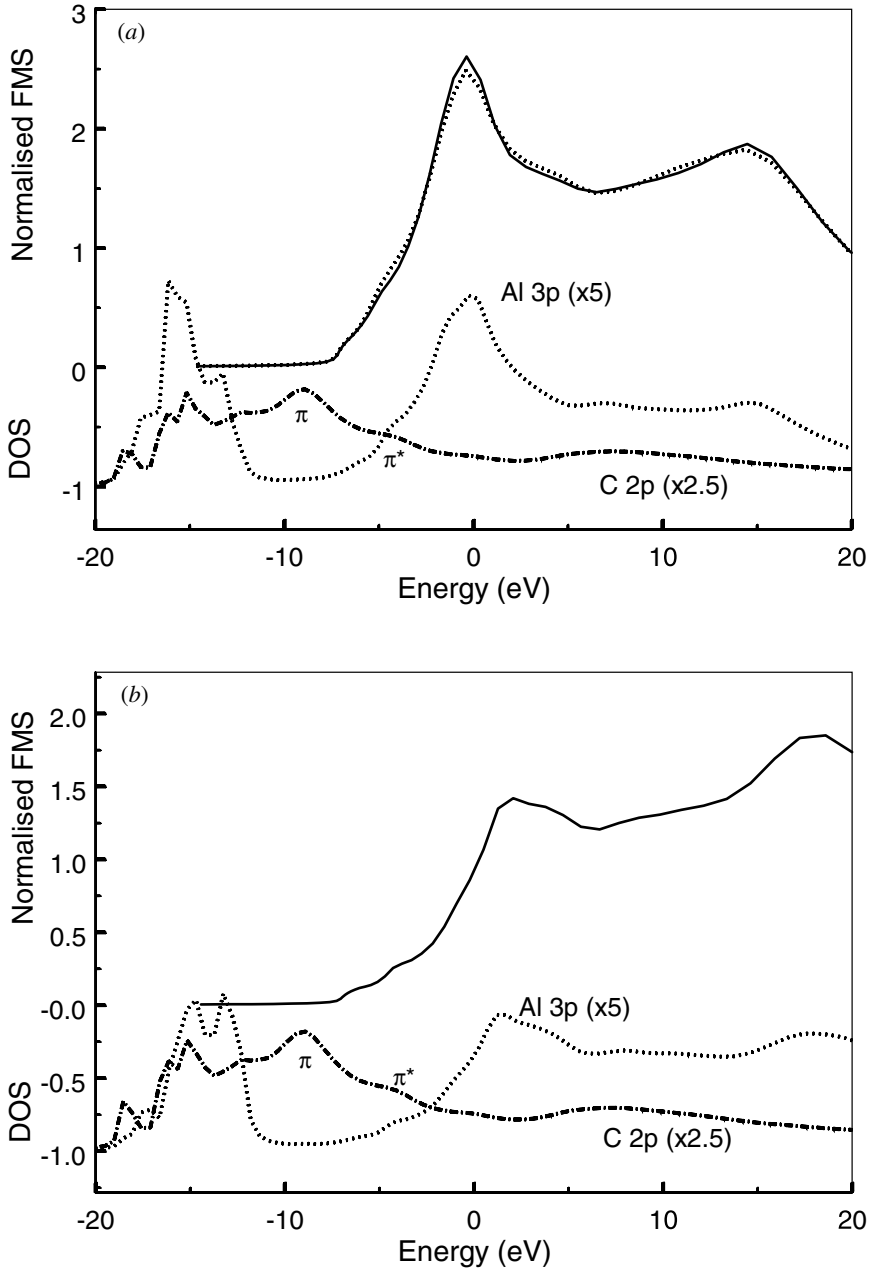

Figure 4. (*a*) FEFF8 cluster calculations on $AlSi_{29}O_{74}(H)$ representing zeolite Beta. At the top the results of SCF FMS calculations are shown. The solid curve is the cluster in the absence of benzene, while the dotted curve is the result of a calculation on a cluster containing benzene adsorbed on the acid site. At the bottom, the calculated aluminium and carbon p DOSs are given (aluminium 3p DOS dotted; carbon 2p DOS dash–dotted). The highest π and lowest π^* orbitals on the carbon are marked. (*b*) FEFF8 cluster calculations on the cluster representing zeolite Beta and including the adsorbate benzene, omitting the core hole. At the top, the SCF FMS calculation is shown. At the bottom, the calculated aluminium and carbon p DOSs are given (aluminium 3p DOS dotted; carbon 2p DOS dash–dotted). The highest π and lowest π^* orbitals on the carbon are marked.

The electron yield spectra also indicate that no change in Al coordination has taken place. Any change in coordination of the Al would be reflected in the near edge by the appearance of characteristic features of the new coordination, while the characteristic tetrahedral features would gradually disappear. One of the characteristic features of tetrahedral Al is the presence of the σ^* peak at $\sim$20 eV. To our knowledge no other Al coordination displays such a distinct peak at this specific energy [2]. Hence, the intensity of this peak can be used as a measure for the disappearance of tetrahedral Al.

An increase in intensity at 2–7 eV (like the increase in the electron yield spectrum of H-Beta/benzene) could indicate the presence of octahedral Al; however, the new intense broad peak most clearly visible in H-Beta/benzene has no fine structure. In general, octahedral Al displays fine structure in the region 5–25 eV above its edge, which is clearly absent in the spectrum of H-Beta/benzene. The high intensity of this broad peak, if due to octahedral Al, would suggest a very large fraction of octahedral Al based on the absorption coefficient [14], and octahedral fine structure would surely be expected in this case. Moreover, an increase in octahedral Al or any other Al coordination should be accompanied by a decrease in tetrahedral Al content. None of the electron yield spectra that display the new broad peak at 5 eV, has a significantly decreased intensity of the 20 eV peak. Thus the electron yield data conclusively indicates that the Al is still mostly tetrahedrally coordinated after the adsorption of the hydrocarbons, with little or no other coordinated Al present, which is in agreement with the fluorescence data.

In conclusion, both detection methods indicate that the Al coordination is unchanged upon molecular adsorption. We confirm that the presence or absence of the broad 5 eV peak is intrinsic to the detection method as proposed in the previous section. In the next section, an explanation is provided for this phenomenon.

4.4. Observation of a Fano resonance

Having established that primarily tetrahedral Al is present in all samples and that no change in coordination around the Al has occurred, we attribute the appearance of the broad feature in the electron yield spectra to the presence of a shake-up satellite feature or Fano resonance (a two-centre, two-electron transition). To understand the nature of this transition, we first discuss the mixing of the aluminum and oxygen orbitals, and the screening of the final-state core hole in Al K-edge XANES spectra for tetrahedral Al.

In spectroscopy, shake-up and shake-down satellite features are well known [15]. They occur in atoms, molecules and solids. Often these final-state satellite features arise from the mono-pole excitation (shake-up) of CT states arising from the sudden turn-on of the core hole potential after absorption of the x-ray photon. Such satellites appear when the core hole–photo-electron attraction (U) is larger than the covalent interaction (Γ) between the absorber atom and the electron source atom (i.e. $U > \Gamma$). This is the case for an aromatic hydrocarbon adsorbed on the acid site in a zeolite. In this case, the transition involves the normal Al 1s to 3p XAS excitation simultaneous with a π (orbital in the aromatic hydrocarbon) to Al 3p CT shake-up to screen the core hole.

In contrast, the covalent interaction between an Al atom and the oxygen atoms surrounding that Al is much larger, so that in this case the reverse is true (i.e. $\Gamma > U$). This is the case at octahedral sites in aluminum oxides, where even though a HOMO–LUMO orbital interaction allows O 2p to Al 3p CT to screen the core hole on Al, no satellites appear. As we discussed previously [5], at a tetrahedral site, the covalent HOMO–LUMO interaction is not allowed by the local symmetry, so that no CT screening occurs at all. When an adsorbate is added, CT occurs from the adsorbate to the Al 3p and screening of the core hole is effective.

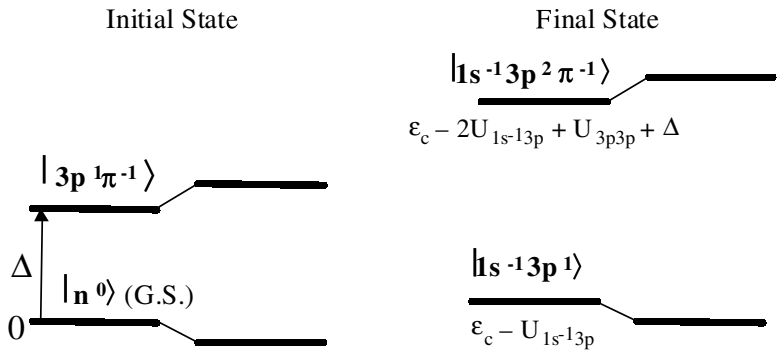

Figure 5. Energy diagram for the initial (ground) state and K-edge XAS final states in the correlated electron model (i.e. when $U > \Gamma$ as discussed in the text). The energies are given for the initial state relative to the unmixed ground state $|n_0\rangle$ (energy = 0), and the final state relative to the unmixed regular core hole excited state $|1s^{-1}3p\rangle$. The energy Δ is the energy required to transfer an electron from the benzene π to the Al 3p (via the benzene π^*). The parameters $U_{1s^{-1}3p^1}$ and U_{3p3p} denote the corresponding Coulomb interaction energies. For both the initial and final states, the premixed state energies are given on the left, and mixed state energies on the right, illustrating the relatively small effects of covalent mixing compared to the correlation effects in this case.

In an XAS experiment, normal resonance peaks occur when the photoelectron is excited into localized antibonding states degenerate with the continuum, i.e. just above the absorption edge. These resonances are called 'shape' resonances because only a single electron, the photoelectron, is involved, and the resonance is determined by the antibonding nature of the orbital, or the 'shape' of the interatomic potential. These shape resonances are often distinguished from true Fano resonances, when more than one electron is involved [16]. When CT occurs, the final state is a two-hole, two-electron state, i.e. the excited photoelectron and the CT electron are together involved in the transition. Thus these CT satellite features may also be referred to as Fano resonances, when they appear above the edge as in this work.

We consider here the case of $U > \Gamma$, the correlated electron model, which is appropriate for say benzene adsorbed on the acidic site in zeolite. In this model, the screening and correlation effects are taken into account first, followed by the covalent interaction. This is the reverse of the more common molecular orbital theory when the covalent interaction is taken into account, and the correlation effects are virtually ignored (which is more appropriate when $\Gamma > U$). Figure 5 shows the energy diagrams for the ground state on the left and the XAS final state on the right. The left side shows the $|n^0\rangle$ (normal or ground state) state correlating to the bottom of the conduction band, where we assign the Fermi level. This level consist of a strongly p–d hybridized Al orbital having a weak covalent interaction with the T_2 symmetry adapted orbitals on the oxygens [5]. As a result of this strong p–d hybridization at a tetrahedral Al site, this orbital immediately above the conduction band minimum is very diffuse. In what follows we shall refer to this level as the Al 3p orbital. At an energy Δ (the CT energy) there is a $|\pi^{-1}3p\rangle$ 'shake-up' state indicating an electron is transferred from the π to the Al 3p orbital. The Al 3p is covalently mixed some with the π^* on the adsorbate and to the extent that this mixing is significant, this shake-up can also be regarded as a π to π^* shake-up. The correlation mixing of the ground level with the $|\pi^{-1}3p\rangle$ level in the initial state can be described by $\psi = a|GS\rangle + b|\pi^{-1}3p\rangle$, where a and b are the correlation mixing coefficients. Here b determines the amount of $|\pi^{-1}3p\rangle$ in the initial ground state, and it is expected to be rather small.

The energy position of the resonance peaks in XANES is determined by the final state, whereas the initial state determines their intensity according to the initial-state, final-state rule [17,18]. A core hole exists in the final state of the absorption process, while a photoelectron is excited into unoccupied orbitals with the correct symmetry. Hence, a core hole photoelectron attraction occurs, deforming the conduction band towards lower energy. This excited $|1s^{-1}3p\rangle$ state (an electron from the 1s is excited into the 3p Al) is shown in figure 5 on the right-hand side. The FEFF8 DOSs shown in figure 4, with and without a core hole, clearly illustrate the deformation of the DOS by the effect of the core hole attraction.

The energy of the normal transition is expressed as

$$h\nu = \varepsilon_c - U_{1s^{-1}3p}, \tag{1}$$

where ε_c is the energy it takes to excite an electron, when no relaxation processes occur. The size of $\boldsymbol{U}_{1s^{-1}3p}$, the core hole–photo-electron attraction, is a function of the screening of the core hole. The less the core hole is screened in the final state, the larger the attraction $\boldsymbol{U}_{1s^{-1}3p}$ will be. As stated, the HOMO–LUMO interaction in T_d Al is forbidden by symmetry, thereby preventing the oxygen CT to screen the core hole on the Al. The XANES final state in tetrahedral Al is therefore unscreened.

In the case of the adsorbates on the acid sites, a CT occurs from the adsorbate to the Al 3p. The excited final state is $|1s^{-1}\pi^{-1}3p^2\rangle$, where two electrons are occupying the 3p orbital in the Al: one core electron is excited from the 1s to the Al 3p and one electron from the π has transferred to the 3p of Al by cost of an energy Δ, and it is now screening the core hole. These two electrons have a mutual repulsion ($\boldsymbol{U}_{3p3p}$) and both feel the attraction of the core hole. The energy of this state is now

$$h\nu = \varepsilon_c - 2U_{1s^{-1}3p} + U_{3p3p} + \Delta. \tag{2}$$

The relative excitation probability into these two final state levels is determined in part by the amount of mixing in the ground state, i.e. the relative magnitudes of a and b and similar mixing in the final state. Assuming the mixing in the final state is indeed very small, the size of a determines the intensity of the $|1s^{-1}3p\rangle$ final state (i.e. normal shape resonance), and b the intensity of the $|1s^{-1}\pi^{-1}3p^2\rangle$ final state (i.e. the Fano resonance). In general b is relatively small and hence the intensity of the Fano transition is expected to be small. This is reflected in the fluorescence spectra, which shows little or no evidence for the Fano resonance. The FEFF8 calculations (figure 4) show that the XAS spectrum is altered just slightly by the presence of the benzene consistent with the absence of an effect in the fluorescence yield spectra.

The screened state, after occurrence of the CT observed in the electron yield spectra (figure 2), can be simulated in an FEFF8 calculation by omitting the core hole during the calculation. Doing so, a distinct different shape of the p DOS is observed (figure 4(*b*)) showing the maximum intensity in the DOS pushed up in energy (equation (2)), with the primary Al 3p peak now falling nearly exactly where the satellite in the electron yield spectrum falls (figure 2) confirming our interpretation. Note that except for the Al 3p 'white line' peak, the remainder of the XAS spectrum appears to be nearly unaffected by the core hole, so the satellite is the only observed evidence of the CT.

The Fano resonance is highly visible in the electron yield data but not in the fluorescence yield data. This occurs because of the different modes of decay of these two final states. Core hole excited states may decay either by fluorescence radiation or by Auger decay, as shown in figure 6. The Auger decay (primarily via KLL or $1s^{-1}$–$2p^{-2}$ decay) suddenly changes the core hole potential (effectively from a charge of 1e to 2e), which can cause final-state shake-off of one or both of the 3p electrons from the Al atom. Such final-state shake-off does not occur in the fluorescence decay (primarily via KL or $1s^{-1}$–$2p^{-1}$ decay), because the effective core hole potential stays the same in this case. This large shake-off of the electrons in the nominal 3p/d

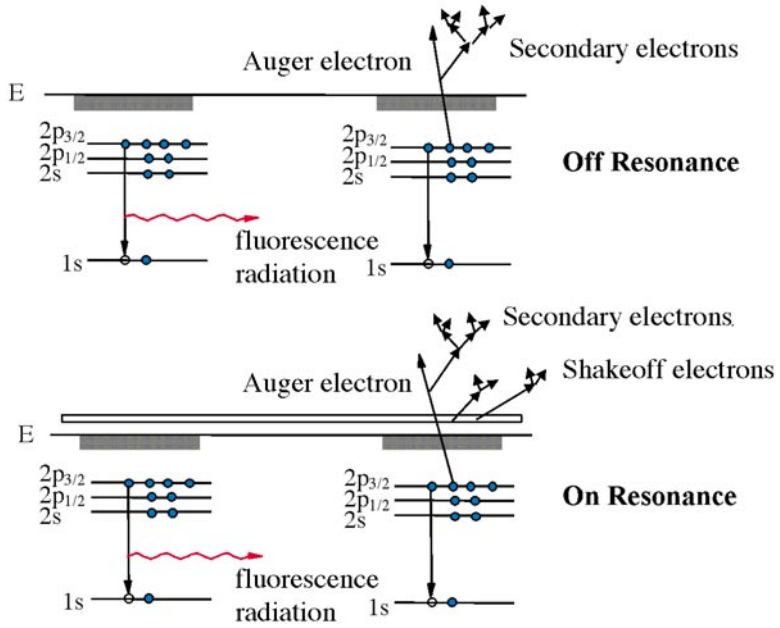

Figure 6. Schematic illustration of the dominant core hole decay processes off resonance (top) and on resonance (bottom) when CT from benzene to Al 3p has occurred. The KL_{23} (1s2p) fluorescence yield is the same for both on and off resonance, but the yield of secondary electrons is magnified on resonance because of the additional shake-off of the two electrons bound in the resonance. Conversely, the 'elastic' $KL_{23}L_{23}$ (1s2p2p) Auger yield is diminished on resonance.

(This figure is in colour only in the electronic version)

orbitals occurs because upon increase of the core hole charge, these diffuse orbitals radially contract. This makes the overlap of the initial and final state 3p/d orbitals much less than unity, and the shake-off probability is directly proportional to this reduction from one [18].

This final-state shake-off magnifies the number of secondary electrons that is detected in the electron yield or in the drain current for this state as illustrated in figure 6. The probability by which fluorescence and Auger decay takes place is fixed, and is tabulated for all accessible K and L edges [19, 20]. For example a Si K core hole (and similarly one in Al) may decay via any of the Auger processes $KL_{23}L_{23}$, $KL_{23}V$, KL_1V and KVV, as well as via x-ray emission, with the following relative rates: 1, 0.002, 0.07, 0.002 and 0.165 respectively [21]. Thus the K core hole decay is dominated by the $KL_{23}L_{23}$ process, followed by the KL_{23} fluorescence process. The $|1s^{-1}3p\rangle$ final state will decay initially via delocalization ($|1s^{-1}3p\rangle$ to $|1s^{-1}\rangle$) of the 3p electron into the continuum (this is what makes this state a 'resonance') followed by normal decay according to the KLL/KL yield ratio with little possibility for shake-off since now essentially no Al 3d–p electrons exists on the atom with the decaying core hole. However, the $|1s^{-1}\pi^{-1}3p^2\rangle$ state is longer lived with respect to electron delocalization (a Fano resonance generally has smaller width than a shape resonance) because of the large correlation energy, U_{3p3p}. Thus, although the contribution of the $|1s^{-1}3p^2\pi^{-1}\rangle$ CT state is low (as given by b), the intensity of this state is magnified in the electron yield, due to the additional shake-off electrons from this state. This shake-off process can be regarded as an intrinsic loss process, supplementing the normal extrinsic loss processes, thus magnifying the total secondary electron yield or drain current for this state. These processes are all illustrated in figure 6.

4.5. CT shake-up and shake-off

The CT shake-up, occurring simultaneously with creation of the core hole via photon absorption, and the shake-off of this electron and/or the photoelectron occurring simultaneously with Auger decay of the core hole, are key to our interpretation of the experimental electron yield data. In this section our results will be compared to charge-transfer shake-up or screening processes known from the literature.

Perhaps the most convincing of the CT shake-up or screening process comes from recent EPR measurements for benzene adsorbed on ZSM-5 zeolite, which directly observe the cation radical $C_6H_6^+$ [22, 23]. These more recent data confirm diffuse reflection spectra of various aromatic compounds, which gave the first evidence of donor–acceptor complexes over oxide catalysts as early as the 1950s [24]. Later, these processes were intensively studied by ESR, where this cation-radical formation was shown to be widespread [25]. The high activity of alumino-silicate systems in this process was found, and zeolites appeared to be even more active [26]. In particular, the benzene cation radical was found on Mordenite and ZSM-5 [27]. Benzene adsorption at 248–298 K on ZSM-5 was found to produce two types of radical, which have been related to cation radicals of benzene monomer and dimer [28]. The high ionization potential of benzene ($I = 9.24$ eV) points to a very strong acceptor centre on the zeolite surface. Photon stimulation revealed a sharp enhancement of the CT process at 2.8 eV and higher [22]. We believe this 2.8 eV can directly be related to our CT energy, Δ, in figure 5. The energy difference between the highest π and Al 3p level in figure 4 is right in the 3–4 eV range.

Observation of the conjugate anion radical centre on oxide systems remains unsolved to this date, although several attempts have been made [22]. Recently however, when illuminating the zeolite with benzene adsorbed at 93 K, a paramagnetic radical pair was found, and these pairs were proposed to have the structure $O_2^- \cdots C_6H_6^+$, which was shown to be an intermediate to the formation of the cation radical. That this radical pair is an intermediate to the formation of the cation radical was confirmed by showing that the benzene cation radical concentration grows linearly with the drop in concentration of the radical pair [22]. Thus it seemed clear that the steps

$$[A_s - C_6H_6] \leftrightarrow [A_s^- - C_6H_6^+] \rightarrow A_s^- + C_6H_6^+$$

occur, where A_s is the strong acceptor site. As a zeolite surface active centre can incorporate chemisorbed molecular oxygen, and the ESR spectra of these radical pairs resemble those of radical pairs with the structure $RO_2^{\bullet} \cdots RO^{\bullet}$, the strong acceptor was proposed to be O_2 [22].

Our interpretation of the XANES results indicates that the acceptor site may simply be the Al atom. An Al atom with a core hole present certainly acts as an acceptor site, as directly indicated by the Fano resonance observed in the electron yield spectra. The required overlap between the initial and final state of the x-ray absorption, as discussed above and illustrated below, suggests that this same Al atom serves as an acceptor site, albeit facilitated by the acidic OH. To our knowledge this is the first direct experimental evidence that the Al atom is directly involved in the electron acceptor site, although it certainly has been suggested many times before [29].

The best evidence supporting the large probability for shake-off of the Al $3p^2$ electrons (i.e. the photoelectron and the CT electron) with Auger decay of the core hole, comes from previously reported Auger and x-ray emission data. This topic has been discussed previously by Turner and Ramaker [30], who presented evidence that the screening CT in all third row XO_4^{n-} type clusters (e.g. SO_4^{2-}, PO_4^{3-} and SiO_2) is primarily of d-like character as found in the current work. The presence of a large peak in the $L_{23}V$ XES spectra for these oxyanions provides good evidence for this, although this peak has been attributed to other less likely sources [31, 32].

The ratio of the total $L_{23}VV$ intensity from similarly prepared Ag_2SO_4 and Ag_2S samples, $I_{SO_4}/I_S = 0.4$, reveals the very large probability for final-state shake-off of the 3d electrons [33]. In the absence of 3d final-state shake-off, this ratio should be one. This 3d final-state shake-off reduces the Auger intensity in the Ag_2SO_4 case, because of the large p–d orbital hybridization that occurs in tetrahedral oxygen coordination as discussed above. Final-state shake-off reduces the total Auger intensity, because as an intrinsic loss process, it takes electrons, which normally would appear in the 'non-scattered' or elastic Auger spectra, and distributes them to lower energy, where they contribute to the secondary electron yield [30]. Thus when the Auger yield is significantly reduced, the secondary electron yield is significantly enhanced, exactly as found in the current work. The observed Auger intensity reduction by a factor greater than 2 in the oxyanions reveals the large magnitude of this effect. Hence the dramatic enhancement in the Fano resonance seen in the electron yield as found in this work is expected, since the Al d orbitals are expected to be even more diffuse than S d orbitals.

4.6. Electron transfer from benzene to Al 3p

Zeolite beta has a three-dimensional pore-channel system. Figure 7(*a*) shows a 12-ring pore of size 6.6×6.7 Å present in zeolite Beta in the [100] direction. In the [010] direction zeolite Beta has another 12-ring pore. These two channels intersect, forming a three-dimensional system. Benzene fits well into pores of these dimensions. Figure 7(*b*) shows schematically an acid site of the zeolite Beta with the benzene adsorbed on it. In general, benzene is adsorbed flat on the pore surface with the benzene π system located on the charge-balancing cations in zeolites [34]. A suggested above, the shake-up could be regarded as a π to π^* shake-up followed by covalent transfer to the diffuse Al 3p orbital. The π^* of the benzene and the radial extent of the T_2 down (3p orbital) on the Al are schematically shown (in fact only one lobe of the p orbital is given). In reality, this orbital also has a covalent overlap with the oxygen orbitals, but for simplicity, this is omitted. The CT or covalent mixing in the ground state could either take place via a direct transfer of an electron onto the Al (through space), or it could occur via the OH group on the zeolite (a concerted transfer).

4.7. Coke formation by 1-hexene on H-Beta

Adsorption of 1-hexene on zeolite H-Beta at room temperature has no effect on either the fluorescence or electron yield data. Several reasons for the absence of the Fano resonance in the hexene case can be given. First, 1-hexene has one double bond, which gives a much larger Δ and the tendency to transfer electrons is small. Second, the hexene might directly react with the acid site on the zeolite, forming an alkoxy species, i.e. a covalent bond is formed between the oxygen and a carbon atom, transforming the double bond into a single C–C bond. The proton of the acidic hydroxyl group is now attached to the carbon next to the oxygen-bonding carbon. Some oligomerization of the hexene might have already taken place at this low temperature, creating aliphatic species inside the pores of the zeolite.

Heating the sample to 250 °C does not lead to any change in the fluorescence or electron yield spectra. However, after the sample is heated to 400 °C, the fluorescence and electron yield spectra are no longer the same. The fluorescence spectrum of H-Beta/1-hexene(400) differs from clean H-Beta and it shows a slight loss of intensity in the white line, and a subsequent increase in intensity at 3–7 eV above the edge. These variations in intensity can be well ascribed to the presence of a small amount of octahedral Al in the sample. Moreover, the fine structure in this spectrum is much less pronounced, which indicates that the medium range order of the tetrahedral Al in this sample is different from the parent sample [8]. The changes

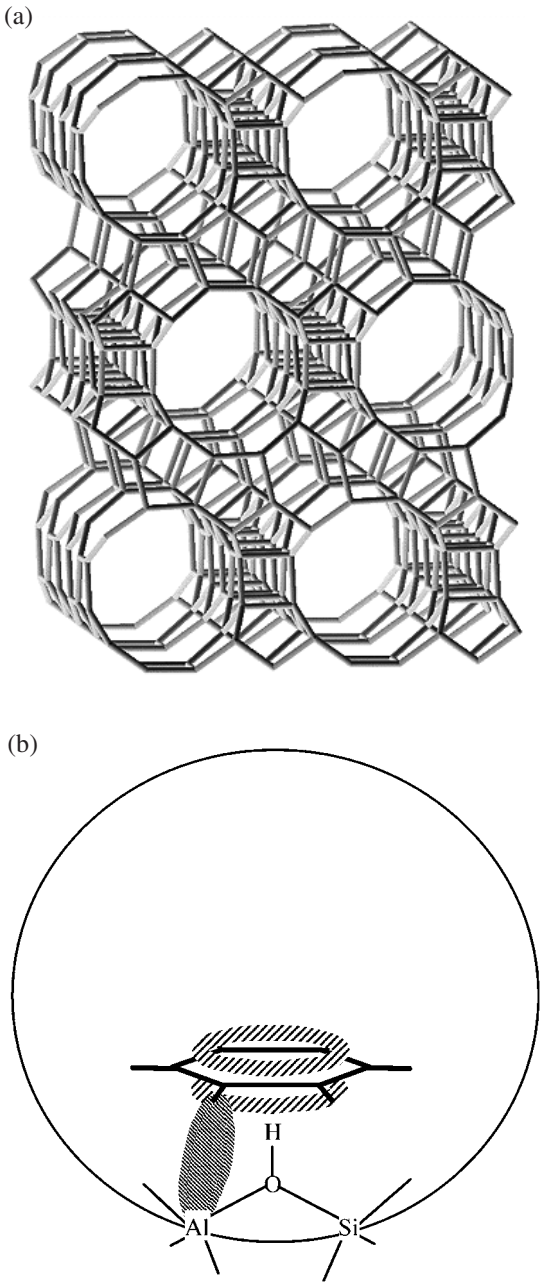

Figure 7. (*a*) 12-membered ring pore-system in the 100 direction in zeolite Beta. A benzene molecule fits nicely in the three-dimensional pore channel system of zeolite Beta. (*b*) Schematic picture of the overlap of the diffuse 3p orbitals on Al with the π^* molecular orbital on the benzene molecule adsorbed on the acid site in the zeolite pore.

in the electron yield spectra are much more obvious. This is attributed to the Fano resonance that occurs due to the presence of aromatic carbon in the near-vicinity of the acid site. It is well known that at temperatures near 400 °C, olefins will form coke [35]. This is also indicated

by the change in colour of this sample, becoming brownish grey. Apparently, some of the 1-hexene is transformed into aromatic coke that is located in the near-vicinity of Al in the framework, creating CT in the XAS spectrum.

The transformation of some tetrahedral Al sites to octahedral sites and a different medium range ordering (figure 3(*a*)) in this sample is an interesting phenomenon. The coke formation might have changed the original tetrahedral Al into octahedral or distorted tetrahedral Al at 400 °C. The octahedral Al could also result from a dealumination process at high temperature due to the presence of some leftover H_2O; however, the shallow bed conditions during this heat treatment would suggest that this did not happen. This phenomenon is not further discussed here, but it will be investigated in more detail later.

5. Conclusions

The adsorption of aromatic hydrocarbons on the acid sites of H-Beta zeolite can be studied at the Al K edge, obtaining both geometric and electronic structure information simultaneously. Conclusions that can be drawn from this study are the following.

(1) Differences between the fluorescence and electron yield data at the Al K edge on the same sample are interpreted by the occurrence of a charge-transfer satellite or Fano resonance. This Fano resonance is detected after adsorption of aromatic molecules on the acid sites in zeolite H-Beta. This two-centre/two-electron transition is only visible using electron yield detection, because the two electrons in the Al 3p orbital can undergo shake-off, which magnifies the electron yield for this state, but leaves the weak transition undetected in fluorescence detection mode.
(2) The occurrence of the Fano resonance is partially determined by the overlap between the T_2(3p) orbitals on the Al and the π^* orbitals on the aromatic molecule, which is a function of the geometrical orientation of the aromatic molecule.
(3) This Fano resonance is believed to be the first solid evidence for the direct role of the Al p–d orbital as the acceptor site, which is suggested to serve as the initial step in the cation–anion radical pair formation.
(4) Using the Fano resonance, coking of 1-hexene on the acid sites of H-Beta can be followed. The Fano resonance appears after heating the sample to 400 °C, indicating aromatic coke is formed on the acid sites of H-Beta.
(5) Indications exist that some Al coordination is changed from tetrahedral to octahedral and/or to some distorted tetrahedral site during the process of coking of 1-hexene at 400 °C.

Acknowledgments

Ad van der Eerden and Dr Andy Smith are gratefully acknowledged for their help during the measurements performed on BL 3.4 at the SRS Daresbury (UK). Jeff Miller is thanked for his interest in these experiments and the provision of part of the samples.

References

[1] Bhatia S 1990 *Zeolite Catalysis: Principles and Applications* (Boca Raton, FL: Chemical Rubber Company) p 1
[2] van Bokhoven J A, Sambe H, Ramaker D E and Koningsberger D C 1999 *J. Phys. Chem.* B **103** 7557
[3] Waychunas G A and Brown G E Jr 1984 *EXAFS and Near Edge Structures III* ed K A Hodgts, B Hedman and J E Penner-Hahn (Berlin: Springer) pp 336–42
Li D, Bancroft G M, Fleet M E, Feng X H and Pan Y 1995 *Am. Mineral.* **80** 432–40
Ildefonse Ph, Kirkpatrick R J, Montez B, Cala G, Flank A M and LagaRde P 1994 *Clays Clay Miner.* **42** 276–87
[4] Cabaret D, Sainctavit P, Ildefonse Ph and Flank A-M 1996 *J. Phys.: Condens. Matter* **8** 3691–704

[5] van Bokhoven J A, Nabi T, Sambe H, Ramaker D E and Koningsberger D C 2001 *J. Phys.: Condens. Matter* **13** 10247–68
[6] Tossell J A 1975 *J. Am. Chem. Soc.* **97:17** 4840–4
Tossel J A 1975 *Chem. Solids* **36** 1273–80
Tossell J A 1973 *Geochim. Cosmochim. Acta* **37** 583–94
[7] Van Bokhoven J A, van der Eerden A M J, Smith A D and Koningsberger D C 1999 *J. Synchrotron Radiat.* **6** 201
[8] Van der Eerden A M J, van Bokhoven J A, Smith A D and Koningsberger D C 2000 *Rev. Sci. Instrum.* **71** 1
[9] Ankudinov A L, Ravel B, Rehr J J and Conradson S D 1998 *Phys. Rev.* B **58** 7565
[10] Bugaev L A, Ildefonse Ph, Flank A-M, Sokolenko A P and Dmitrienko H V 1998 *J. Phys.: Condens. Matter* **10** 5463–73
[11] Kunkeler P J, Zuurdeeg B J, van der Waal J C, van Bekkum H, van Bokhoven J A and Koningsberger D C 1998 *J. Catal.* **180** 234
[12] Jones R G and Woodruff D P 1982 *Surf. Sci.* **114** 38
[13] Norberg V and Su B-L 1998 *Proc. 12th Int. Zeolite Conf.* ed M M J Treacy, B K Marcus, M E Bisher and J B Higgins (Warrendale, PA: Materials Research Society)
[14] Shimizu K I, Kato Y, Yoshida T, Yoshida H, Satsuma A and Hattori T 1999 *Chem. Commun.* 1681
[15] van der Laan G, Zaanen J, Sawatzky G A, Karnatak R and Esteva J-M 1986 *Phys. Rev.* B **33–6** 4253
D'Addato S, Ramaker D E, Cosso R, Gregory D, Morrison T P, Unsworth P, Duò L, Panaccione G, Nannarone S and Weightman P 1994 *Europhys. Lett.* **26** 85
Sambe H, Qian X and Ramaker D E 1996 *Phys. Rev.* B **53–4** 1779
Stern E A 1982 *Phys. Rev. Lett.* **49–18** 1353
[16] Fano U and Cooper J 1975 *Phys. Rev.* A **246** 555
[17] von Barth U and Grossman G 1979 *Solid State Commun.* **32** 645
von Barth U and Grossman G 1980 *Phys. Scr.* **21** 580
von Barth U and Grossman G 1982 *Phys. Rev.* B **25** 5150
von Barth U and Grossman G 1983 *Phys. Scr.* **28** 107
[18] Ramaker D E 1982 *Phys. Rev.* B **25** 7341
[19] Chen M H, Crasemann B and Mark H 1970 *At. Data Nucl. Data Tables* **24** 13
Chen M H, Crasemann B and Mark H 1980 *Phys. Rev.* A **21** 436
[20] Babenkov M I, Bobykin B V and Zhdanov V S 1983 *J. Electron Spectrosc. Relat. Phenom.* **31** 307
[21] Ramaker D E, Hutson F L, Turner N H and Mei W N 1986 *Phys. Rev.* B **33** 2574
[22] Volodin A M, Bolshov V A and Konovalova J T A 1994 *Mol. Eng.* **4** 201
[23] Feldman V I, Sukhov F, Orlov A, Kadam R, Itagaki Y and Lund A 2000 *Phys. Chem. Chem. Phys.***2** 29
[24] Terenin A and Sidorova V 1950 *Dokl. Akad. Nauk. SSSR. Ser. Khim.* **2** 152
[25] Fogo J K 1961 *J. Phys. Chem.* **65** 1919
Terenin A, Barachevsky V, Kotov E and Kolmogarov V 1963 *Spectrochim. Acta* **19** 1797
Rooney J J and Pink R C 1962 *Trans. Faraday Soc.* **62** 730
Stamirez D N and Turkevich J 1964 *J. Am. Chem. Soc.* **86** 749
Teterin A 1965 *J. Chim. Phys.* 646
Flockart B D, Scotl J A N and Pink R C 1966 *Trans. Faraday Soc.* **62** 730
[26] Bard A J, Ledwith A and Shine H J 1976 *Adv. Phys. Org. Chem.* **13** 155
Loktev M B and Slinkin A A 1976 *Usp. Khim.* **45** 1594
[27] Kurita Y, Sonada T and Sato M 1970 *J. Catal.* **19** 82
Vedrine J C, Auroux A, Bolis V, Dejaifve P, Naccache G, Wierzchowski P, Derouane E G, Nagy J B, Gilson J-P, van Hooff J H C, van den Berg J P and Wolthuizen J 1979 *J. Catal.* **59** 248
Kucherov A V, Slinkin A A, Kondraryev D A, Bondarenko T N, Rabinstein A M and Manachev Kh M 1986 *J. Mol. Catal.* **37** 107
[28] Varter M K and Vincow G 1967 *J. Chem. Phys.* **47** 292
Edlung O, Kinel P-O, Lund A and Shimizu A 1967 *J. Chem. Phys.* **46** 3679
[29] Zhidomirov G M and Kazansky V B 1986 *Adv. Catal.* **34** 131
[30] Turner N H and Ramaker D E 1983 *J. Vac. Sci. Technol.* A **1** 1229
[31] Henke B L and Taniguchi L 1976 *J. Appl. Phys.* **47** 1027
[32] Griscom D L 1977 *J. Non-Cryst. Solids* **24** 155
[33] Turner N H, Murday J S and Ramaker D E 1980 *Anal. Chem.* **52** 84
Turner N H, Murday J S and Ramaker D E 1980 *J. Vac. Sci. Technol.* **17** 214
[34] Su B L 1997 *J. Chem. Soc. Faraday Trans.* **93** 1449
[35] Snape C E, McGhee B J, Martin S C and Andresen J M 1997 *Catal. Today* **37** 285